Dalton Transactions

Accepted Manuscript

This is an *Accepted Manuscript*, which has been through the RSC Publishing peer review process and has been accepted for publication.

Accepted Manuscripts are published online shortly after acceptance, which is prior to technical editing, formatting and proof reading. This free service from RSC Publishing allows authors to make their results available to the community, in citable form, before publication of the edited article. This *Accepted Manuscript* will be replaced by the edited and formatted *Advance Article* as soon as this is available.

To cite this manuscript please use its permanent Digital Object Identifier (DOI®), which is identical for all formats of publication.

More information about *Accepted Manuscripts* can be found in the **Information for Authors**.

Please note that technical editing may introduce minor changes to the text and/or graphics contained in the manuscript submitted by the author(s) which may alter content, and that the standard **Terms & Conditions** and the **ethical guidelines** that apply to the journal are still applicable. In no event shall the RSC be held responsible for any errors or omissions in these *Accepted Manuscript* manuscripts or any consequences arising from the use of any information contained in them.

Journal Name

RSCPublishing

ARTICLE

Solution-phase catalytic synthesis, characterization and growth kinetics of Ag_2S-CdS matchstick-like heteronanostructures

Cite this: DOI: 10.1039/x0xx00000x

Received 00th January 2012,
Accepted 00th January 2012

DOI: 10.1039/x0xx00000x

www.rsc.org/

Junli Wang,*[ab] Hui Feng,[a] Kangmin Chen,[c] Weiling Fan[a] and Qing Yang*[b]

A facile catalytic growth route was developed for the low-temperature solution synthesis of Ag_2S-CdS matchstick-like heteronanostructures in oleylamine, which are composed of Ag_2S spherical head and CdS rod-like stem. Ag_2S nanoseeds acted as an effective catalyst for the growth of CdS nanorods and remained at the tip of the resultant nanorods, leading to the formation of Ag_2S-CdS heterostructures with a matchstick shape. The diameter of Ag_2S heads and the length of CdS stems could be easily controlled by varying the molar ratios of Ag/Cd precursors. The differential scanning calorimetry (DSC) and variable-temperature X-ray diffraction (XRD) studies confirmed that Ag_2S catalytic seeds underwent a phase change, that is, they were in the high-temperature superionic conducting cubic structure during the CdS nanorod growth and then converted to the low-temperature monoclinic crystal structure as the reaction was cooled to room temperature. The influence of synthetic temperature on the product morphology was investigated and the morphological evolution at different growth stages was monitored using transmission electron microscopy (TEM). Furthermore, the growth kinetics of Ag_2S-CdS matchstick-like heteronanostructures, including the dissolution, nucleation and growth of CdS within Ag_2S catalyst, was reasonably discussed on the basis of the structural characteristics of superionic cubic Ag_2S catalyst and the low solubility of CdS in Ag_2S derived from Ag_2S-CdS binary phase diagram.

1. Introduction

Combining two or more chemically dissimilar components into one single nanostructure, i.e., heterostructured nanocrystals, is an effective method to construct functional nanomaterials with integrated and/or enhanced optical, electrical, magnetic, and catalytic properties.[1–7] Owning to these physical and chemical properties being shape- and composition-dependent, many efforts have been devoted to the control over heterostructured nanocrystals with various materials and morphologies. For example, the two-component heteronanostructures composed of metal-metal,[3] metal-metal oxide,[4] metal-semiconductor,[5,8] metal oxide-semiconductor,[6,9] and semiconductor-semiconductor,[7,10–17] have been successfully prepared and they exhibit a large range of morphologies and structures, including the spherical, polyhedral or rod-like core/shell shape,[3,6,8,10,11] asymmetric dimer shape,[4,9,12] Janus-like shape,[13] one-dimensional (1D) axial or radial wire-like shape (i.e., nanowire heterostructures),[14–16] and matchstick-like shape.[5,7,17] In recent years, there is a growing interest in the tunable preparation of matchstick-like heteronanostructures,[5,7,17] in which the spherical nanocrystals of one material act as the head section and the 1D nanorods of the other material as the stem section. The vital issue to construct matchstick-like heteronanostructures is how to realize the combination of these two sections without the yield of isolated particles.

One synthetic strategy is to use 1D nanorods as seeds and then grow the nanocrystals of the second material onto one apex of these nanorods. This strategy is generally conducted in the solution chemistry and there are two mechanisms that can explain the formation of matchstick-like morphology. One mechanism is that the crystallographic facets at one end of nanorods have much higher reactivity than those at side surfaces and the other end, which enables the growth of the second material at the high active end of the nanorods. The preparation of Au-tipped CdSe nanorod,[5] PbSe-tipped CdS nanorod[17] and Co-tipped CdSe@CdS nanorod[18] heterostructures was achieved by this mechanism. The heteroepitaxial growth of the second material on the facets at the end of nanorods, based on a proper lattice match between certain crystallographic facets of two materials, is the other mechanism that can allow the yield of matchstick-like

heteronanostructures, such as Fe_xO_y-tipped TiO_2 nanorod heterostructures.[19]

An alternative strategy to prepare matchstick-like heteronanostructures is to use spherical (or nearly spherical) nanocrystals as seeds and induce the growth of nanorods on them. The spherical nanocrystals can induce the heteroepitaxial growth or catalytic growth of 1D nanorods of the second material and then remain on the end of the resulting nanorods, which will produce matchstick-like heterostructured nanocrystals. For example, Cu_2S nanocrystals were used as seeds for the epitaxial growth of ZnS, In_2S_3, $CuInS_2$ and $CuInZnS_x$ nanorods,[20–22] in which the seeds and the growing nanorods have good matches in the crystal structure and lattice constants and accordingly the matchstick-like heteronanostructures of Cu_2S-ZnS, Cu_2S-In_2S_3, Cu_2S-$CuInS_2$ and Cu_2S-$CuInZnS_x$ were obtained. Meanwhile, nonstoichiometric copper sulfide $Cu_{1.94}S$ nanocrystals were also reported to be used in the synthesis of Cu_2S-In_2S_3 and $Cu_{1.94}S$-ZnS matchstick-like heterostructured nanorods.[23–25] In these reports, $Cu_{1.94}S$ nanocrystals were proposed as catalysts in the growth of In_2S_2 and ZnS nanorods, where the heteroepitaxial growth was also involved based on the results of high-resolution transmission electron microscopy (HRTEM).[23–25] Recently, Ag_2S nanocrystals, which could catalyze the growth of ZnS nanowires or nanorods,[26,27] have been used to synthesize Ag_2S-ZnS, Ag_2S-CdS and Ag_2S-$AgInS_2$ matchstick-shaped heteronanostructures.[7,27–29]

As for a catalytic growth mechanism conducted in either high-temperature vapor or low-temperature solution phase, the catalyst particles usually remain at the tip of the resultant nanowires or nanorods,[14–16,23–28,29a,b] which offers us a handy route for the preparation of matchstick-shaped heteronanostructures. In our recent work,[30] we reported the solution-phase synthesis of ZnS, CdS, ZnSe and CdSe nanowires or nanorods using Cu_2S, Ag_2S and Ag_2Se nanocrystals as catalysts. Different from the liquid-state catalysts in the vapor–liquid–solid (VLS)[14,15] or solution–liquid–solid (SLS)[16] mechanism, we found that Cu_2S, Ag_2S and Ag_2Se catalysts were in their solid-state superionic conductor phase during the nanowire/nanorod growth and therefore we proposed a solution-solid-solid (SSS) catalytic mode to elucidate the nanowire/nanorod formation. By using the SSS growth mechanism, some matchstick-like heteronanostructures containing two dissimilar components, such as Cu_2S-ZnS, Cu_2S-CdS, Ag_2S-CdS and Ag_2S-ZnSe,[30] could been prepared. In this study, we specifically demonstrate the tunable synthesis, detailed characterization and growth kinetics of Ag_2S-CdS matchstick-like heteronanostructures, which are made of a spherical Ag_2S catalytic head and a rod-like CdS stem. The studies on the phase transition behaviors of Ag_2S catalytic heads by means of differential scanning calorimetry (DSC) thermal analysis and variable temperature X-ray powder diffraction (XRD) confirmed that high-temperature superionic conducting state Ag_2S[31,32] catalyze the CdS nanorod growth and thus produce Ag_2S-CdS matchstick-like heteronanostructures. These heteronanostructures integrate wide band gap semiconducdtor CdS (bulk E_g = 2.5 eV)[13] with narrow band gap semiconductor Ag_2S (bulk E_g = 0.9−1.1 eV),[33,34] which exhibit a type I (sandwiched) electronic band alignment and may find their potential use in many optical and optoelectronic fields.[34]

2. Experimental

2.1. Synthesis of Ag_2S-CdS matchstick-like heteronanostructures.

The matchstick-shaped heteronanostructures of Ag_2S-CdS could be prepared by a one-pot two-step synthesis procedure using Ag_2S nanocrystals as seeded catalyst. The first step is to prepare Ag_2S nanocrystals. In a typical procedure, a certain amount of $AgNO_3$ (0.05−0.2 mmol, 8.5−34 mg) and S powder (0.25 mmol, 8 mg) were added into 8 mL oleylamine (Aladdin, 80–90%) in a 25 mL two-necked flask under stirring, and the mixture solution was heated to 160 °C and reacted at this temperature for 20 min to synthesize Ag_2S nanocrystals. Then, 0.2 mmol $Cd(DDTC)_2$ (Cd $(S_2CNEt_2)_2$, 82 mg) was swiftly added into the above reaction solution and kept at 160 °C for 45 min. The solid products were collected by centrifugation, washed with dichloromethane and ethanol three times, and then dried in a vacuum at 50 °C for further characterization. The Cd precursor, $Cd(DDTC)_2$, was prepared according to the method described previously.[7,29] The diameter of Ag_2S nanocrystals and the length of CdS nanorods in the Ag_2S-CdS matchstick-shaped heteronanostructures could be tuned by varying the molar ratio of Ag/Cd precursors from 1:1, 1:2 to 1:4. Ag_2S nanocrystals could be synthesized in a large scale through the reaction between $AgNO_3$ and S. For example, 1 mmol $AgNO_3$ and 2 mmol S powder can lead to an increased amount of Ag_2S nanocrystals large enough for the XRD and DSC characterization. All of syntheses did not need the protection of inert gas (e.g., Ar and N_2).

2.2. Characterization.

Room temperature X-ray powder diffraction (XRD) was collected on a Bruker D8 Advance X-ray diffractometer with Cu K_α radiation (λ= 1.54184 Å) at a voltage/current of 40 kV/40 mA, scan rate of 2° min^{-1} and a step size of 0.02°. Variable temperature XRD data were collected using Shimadzu XRD-7000 with Cu K_α radiation (λ = 1.54187 Å). Transmission electron microscopy (TEM) and high-resolution TEM (HRTEM) images were performed on a JEOL JEM 2010 TEM at an acceleration voltage of 200 kV. High-angle annular dark field scanning TEM (HAADF-STEM) images and line-scan energy-dispersive X-ray spectroscopy (EDS) were carried out on a JEOL JEM 2010F field-emission TEM at 200 kV, equipped with an X-ray energy dispersive spectrometer (EDS, Oxford Inca). X-ray photoelectron spectroscopy (XPS) analyses were carried out on a VGESCA-LAB MKII X-ray photoelectron spectrometer with an $Al_{K\alpha}$ excitation source (1486.6 eV). Differential scanning calorimetry (DSC) measurements were performed on NETZSCH DSC 204 in the range 0–200 °C with a heating/cooling rate of 5 °C min^{-1}.

3. Results and discussion

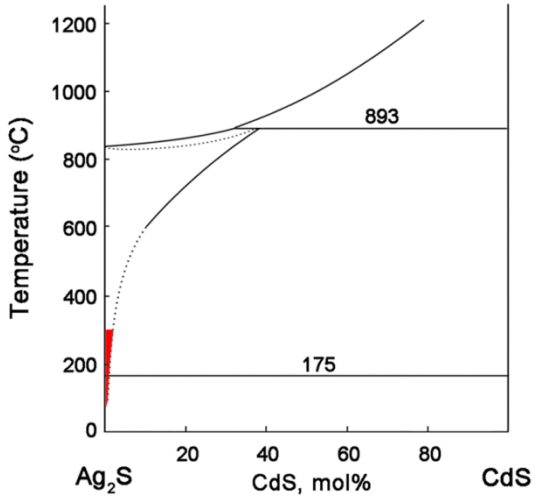

Fig. 1 Schematic of binary Ag_2S-CdS phase diagram.[36]

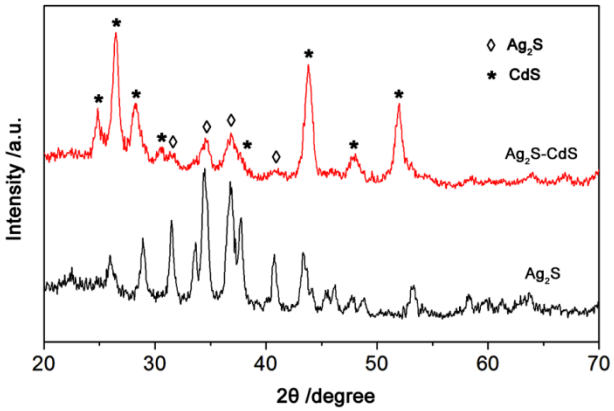

Fig. 2 XRD patterns of the Ag_2S-CdS matchstick-shaped heteronanostructures (red line) and the pure Ag_2S nanocrystals (black line).

In the experiments, Ag_2S nanocrystals were prepared in advance through the reaction of $AgNO_3$ with S power in oleylamine at 160 °C and then used as seeds to catalyze the growth of CdS nanorods. Oleylamine acted as multifunctional roles of solvent, surfactant and reductant.[35] Single-source molecular precursor, $Cd(S_2CNEt_2)_2$ ($Cd(DDTC)_2$), was used as Cd and S sources for the synthesis of CdS nanorods.[29c] As a catalyst, Ag_2S nanoseeds will remain at one end of CdS nanorods as their growth is finished, so that matchstick-like Ag_2S-CdS heteronanostructures can be prepared through this process. After reexamining the phase diagram of Ag_2S-CdS binary system (Fig. 1),[36] we can find that CdS has a low solubility in Ag_2S from a simple extrapolation of the bulk solubility to the low temperature region of 100–300 °C (the red region in Fig. 1). The low solubility of CdS in Ag_2S not only enables Ag_2S nanocrystals to be a good candidate catalyst for the growth of 1D CdS nanorods or nanowires, but also favors the dissolution, nucleation and phase extraction of CdS within Ag_2S nanocrystals. Similar cases relevant to the solubility have been demonstrated for the growth of nanowires/nanorods by a catalytic mechanism derived from an inorganic compound or metal catalyst.[23,27,30,37–39] At the same time, a proper dissolution of CdS in Ag_2S can allow a good combination of CdS and Ag_2S into a single structure, which can effectively prevent the self-nucleation and growth of CdS and therefore inhibit the yield of CdS and Ag_2S isolated nanoparticles. On the other hand, 100–300 °C is a very suitable temperature range for the solution-phase synthesis of nanomaterials in consideration of the boiling points of many common solvents.

Fig. 2 shows the X-ray diffraction (XRD) patterns of the resultant Ag_2S-CdS matchstick-like heteronanostructures and the pure Ag_2S nanocrystals, respectively. The heteronanostructures are prepared from a 1:2 molar ratio of Ag/Cd precursors and it can be seen from the XRD pattern that they are made of crystalline phases of CdS and Ag_2S (the red line in Fig. 2). In detail, the diffraction peaks from CdS in both zinc blende (ZB, JCPDS# 89-0440) and wurtzite (W, JCPDS# 75-1545) structures are detected. The ZB and W phase CdS has an approximate 60%:40% molar ratio. The peaks at 2θ 31.6 (d = 2.85 Å), 34.5° (d = 2.60 Å), and 36.8 (d = 2.44 Å) are in good agreement with the characteristic peaks of monoclinic Ag_2S (JCPDS# 89-3840, a = 4.23 Å, b = 6.91 Å, and c = 7.87 Å), corresponding to the (-112), (-121), and (121) planes. The monoclinic structure of Ag_2S is further verified by the XRD measurement recorded on the pure Ag_2S nanocrystals prepared under similar conditions (the black line in Fig. 2). The Ag_2S-CdS matchstick-like heteronanostructures prepared from 1:4 Ag/Cd molar ratio have a similar XRD pattern to those prepared 1:2 Ag/Cd molar ratio, which is indexed in detail in the Supplementary Information (ESI†, Fig. S1).

The transmission electron microscopy (TEM) studies directly confirm the formation of Ag_2S-CdS matchstick-shaped heteronanostructures. As shown in Fig. 3, each heterostructured nanocrystal has a darker spherical head and a brighter rod-like stem, which is typically in a matchstick-like morphology. The difference in the contrast suggests that the two parts are composed of different materials, which are proven (shown below) to be Ag_2S head and CdS stem, respectively. Interestingly, the diameter of Ag_2S head and the length of CdS stem could be tunable just by varying the molar ratios of Ag/Cd precursors. At the 1:1 Ag/Cd molar ratio, the average length of CdS stems is 24.2 nm and the average diameter of Ag_2S heads is 14.7 nm (Fig. 3a,b). At the 1:2 Ag/Cd molar ratio, the average length of CdS stems is 34.6 nm and the average diameter of Ag_2S heads is 17.6 nm (Fig. 3c,d). When the Ag/Cd molar ratio is changed to 1:4, the CdS stems have a mean length of 68.4 nm and the Ag_2S heads a mean diameter of 15.7 nm (Fig. 3e,f). These data were extracted from 80 Ag_2S-CdS matchstick-like heteronanostructures. It is notable from these TEM images that CdS stems have a diameter slightly smaller (~1−4 nm) than the corresponding Ag_2S heads at the junction region (Fig. 3).

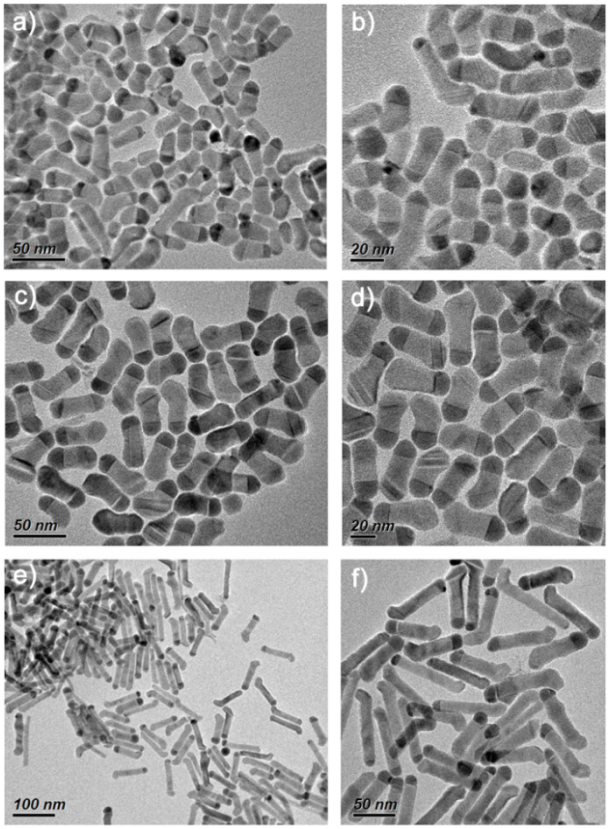

Fig. 3 TEM images of Ag_2S-CdS matchstick-shaped heteronanostructures prepared at different Ag/Cd molar ratios: (a,b) 1:1, (c,d) 1:2, and (e,f) 1:4. The amount of $Cd(DDTC)_2$ is fixed as 0.2 mmol while that of $AgNO_3$ ranges from 0.2, 0.1 to 0.05 mmol.

A high-angle annular dark field scanning TEM (HAADF-STEM) image of the as-synthesized heteronanostructures (Fig. 4a) reveals a clear contrast between the head and the stem, which hints that the heteronanostructures are composed of two different materials. Their chemical compositions were measured by the line-scan energy-dispersive spectroscopy (EDS). As displayed in Fig. 4b, the EDS elemental profiles clearly reveal the distribution of Ag, Cd and S elements in the heterostructures: Ag is limited to the head part and Cd to the stem part, while S is distributed throughout two parts. The calculated Ag:S and Cd:S elemental ratios are approximately 2:1 and 1:1, respectively. On the basis of the EDS analyses coupled with the XRD results, a conclusion can be reached that the matchstick-shaped heteronanostructures indeed consist of Ag_2S head and CdS stem.

High-resolution TEM (HRTEM) was further used to characterize the Ag_2S-CdS heteronanostructures. The well-defined lattice fringes in the HRTEM image suggest good crystallinity of both CdS stem and Ag_2S head (Fig. 5). For the Ag_2S head, the distance measured between two adjacent fringes is 6.92 Å, which is in good agreement with the interfacial spacing of the monoclinic Ag_2S (010) planes, and the corresponding fast Fourier transform (FFT) pattern contains the diffraction spots from the (010) and (001) planes of monoclinic phase Ag_2S (JCPDS# 89-3840). The HRTEM image of CdS stem shows the single crystal nature of CdS nanorod and its FFT pattern can be indexed as the [1-10] zone axis diffraction pattern of cubic ZB phase CdS. The measured adjacent fringe distance in the HRTEM image is 3.37 Å, corresponding to the interplanar spacing of cubic CdS(111) planes.

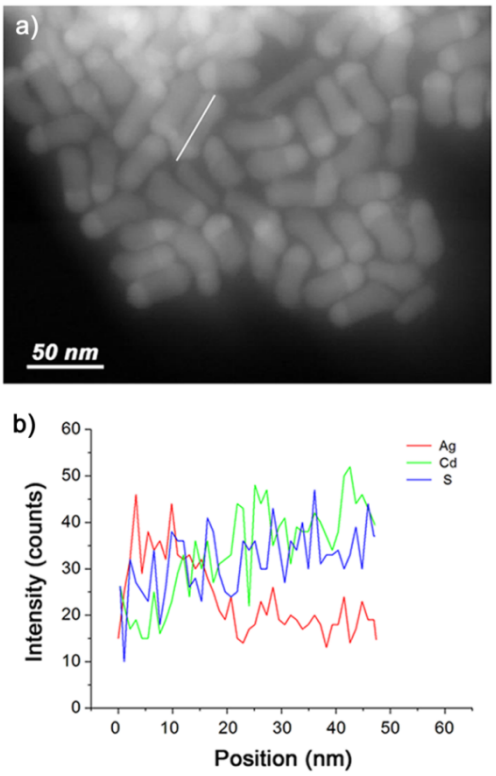

Fig. 4 (a) HAADF-STEM image and (b) Line-scan EDS elemental profiles of Ag, Cd and S of Ag_2S-CdS matchstick-shaped heteronanostructures prepared at 1:2 Ag/Cd molar ratio. The EDS line scan was recorded along the white line shown in panel (a).

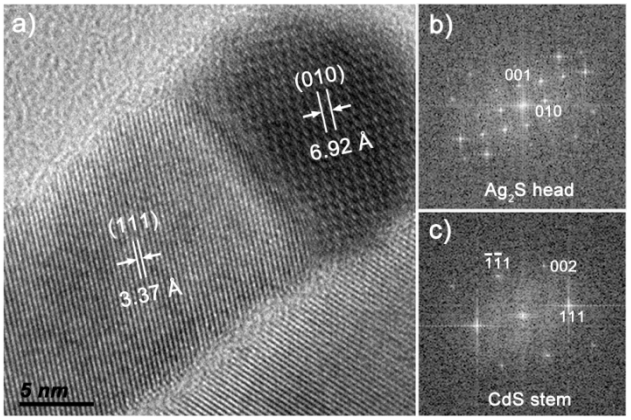

Fig. 5 (a) A typical HRTEM image of the as-prepared Ag_2S-CdS matchstick-shaped heteronanostructures and its corresponding FFT patterns for (b) the Ag_2S head and (c) the CdS stem, respectively.

The above results of XRD, TEM, EDS and HRTEM studies confirm that the as-obtained heteronanostructures are composed of Ag_2S heads and CdS nanorods, which display a matchstick-like shape. It has been reported that, besides the Ag_2S-CdS

Journal Name RSCPublishing

ARTICLE

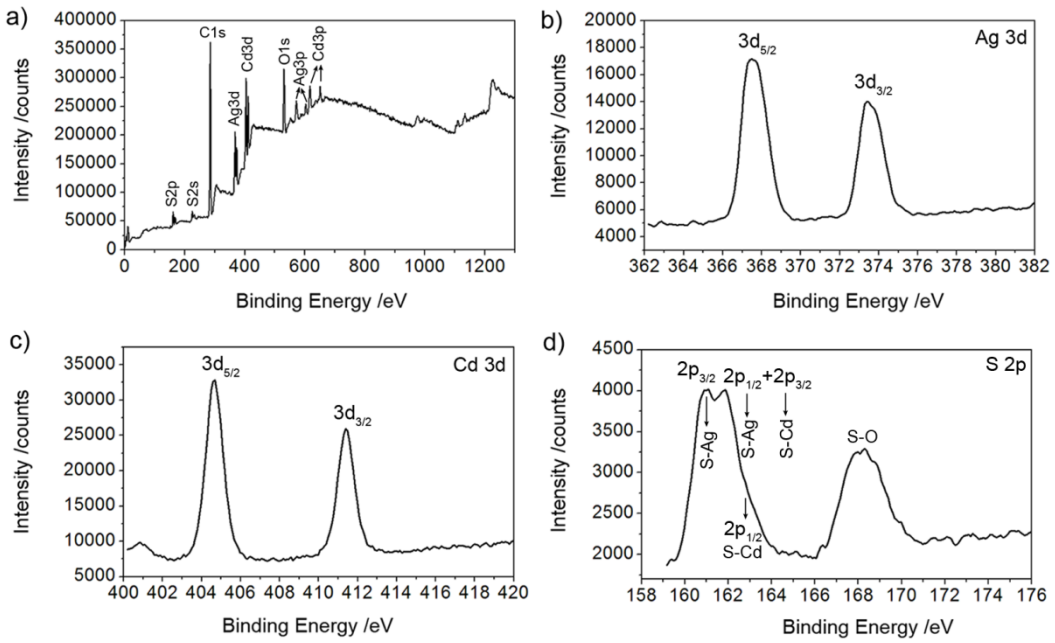

Fig. 6 XPS spectra of Ag_2S-CdS matchstick-like heteronanostructures prepared at 1:2 Ag/Cd molar ratio: (a) Survey spectrum; (b–d) High-resolution spectra of Ag 3d, Cd 3d and S 2p core levels, respectively.

heteronanostructures, Ag_2S nanocrystals were also used to synthesize Ag_2S-ZnS and Ag_2S-$AgInS_2$ matchstick-shaped heteronanostructures as well as ZnS nanowires, where Ag_2S is an excellent catalyst for the growth of 1D nanorods or nanowires.[7,26–30] Recently, however, Li et al. reported the use of Ag nanocrystals as seeds for the synthesis of Ag-ZnS metal-semiconductor nanorod heterostructures.[40] X-ray photoelectron spectroscopy (XPS) is an accurate technique to discriminate the oxidation state of an element. In this work, XPS spectra were taken to determine the valence state of Ag and the chemical composition (purity) in the Ag_2S-CdS matchstick-like heteronanostructures. As shown in Fig. 6a, the XPS survey spectrum reveals the presence of C 1s, O 1s, Ag 3d, Cd 3d and S 2p core level peaks, confirming the high purity of the sample only consisting of Ag, Cd and S. In the high-resolution XPS spectrum of Ag 3d core level (Fig. 6b), the $3d_{5/2}$ and $3d_{3/2}$ peaks are loaded at 367.5 eV and 373.4 eV, respectively, which match well with those from Ag_2S.[33,41–43] Such a result shows that the oxidation state of Ag in the Ag_2S-CdS matchstick-like heteronanostructures is univalent and thus excludes the existence of elemental metal Ag (zero valent) in the sample, consistent with the above XRD analyses (Fig. 2). At the same time, the amount of S powder is excessive in the experiments for synthesizing Ag_2S catalyst seeds, which ensures the yield of Ag_2S without metal Ag.

Shown in Fig. 6c is the high-resolution XPS spectrum for the Cd 3d core level. The $3d_{5/2}$ signal at 404.7 eV and $3d_{3/2}$ at 411.5 eV are detected, which agree well with Cd 3d core levels from CdS.[41] Interestingly, the S 2p high-resolution XPS spectrum provides rich chemical information to show the coexistence of Ag_2S and CdS in the heteronanostructures. Three obvious peaks are detected in the spectrum (Fig. 6d). The peak at 160.8 eV is assigned to the S $2p_{3/2}$ binding energy from Ag_2S.[33,41] Its corresponding spin-orbit splitting peak is the S $2p_{1/2}$ peak, which is measured at 161.9 eV in the XPS spectrum, showing a 1.1 eV higher than the S $2p_{3/2}$ peak in binding energy. However, the peak intensity ratio of S $2p_{1/2}$ to S $2p_{3/2}$ measured in our XPS study is larger than that in the pure Ag_2S[33] or in the standard XPS spectrum for S 2p core level.[42] Such an intensity enhancement is due to the overlap of the S $2p_{1/2}$ peak from Ag_2S with the S $2p_{3/2}$ peak from CdS (Fig. 6d). As shown in the literature,[43] the S 2p core level in CdS has a higher binding energy ~1.0 eV than the S 2p core level in Ag_2S. The binding energy of the S $2p_{3/2}$ peak from CdS is higher by 1.0 eV than the binding energy of the S $2p_{3/2}$ peak from Ag_2S and just overlaps with the S $2p_{1/2}$ peak from Ag_2S. Meanwhile, the peak overlapping also causes a broadening for the S 2p core level

peak in the XPS spectrum (Fig. 6d). A relatively weak shoulder peak is also detectable at the higher energy side of this overlapped peak and it can be indexed to the S $2p_{1/2}$ core level from CdS with a binding energy of 162.8 eV (Fig. 6d). It is notable that there is a broad peak centered at 168.2 eV in the high-resolution XPS spectrum of S 2p core level, which is derived from the oxidized S (S-O)[41,43] on the surface of Ag_2S-CdS matchstick-like heteronanostructures.

It has been reported that Ag_2S, either in the bulk or nanoscale form, displays a solid-solid phase transition at ~180 °C[31,32,44,45] from low-temperature monoclinic-structured semiconductor to high-temperature cubic-structured superionic conductor, which is reversible and illustrated in Fig. 7a. In the Ag_2S-CdS phase diagram shown in Fig. 1, this phase transition of Ag_2S is indicated with the solidus line at 175 °C,[36] being a little lower than the transition temperature (~180 °C) of Ag_2S reported by other researchers.[44,45] The differential scanning calorimetry (DSC) thermal analysis technique is an effective tool for studying the structural phase change of Ag_2S.[44,45] In this work, we used DSC technique to contrastively investigate the phase transition behaviors of the as-prepared pure Ag_2S nanocrystals and the Ag_2S catalyst heads from Ag_2S-CdS matchstick-like heteronanostructures.

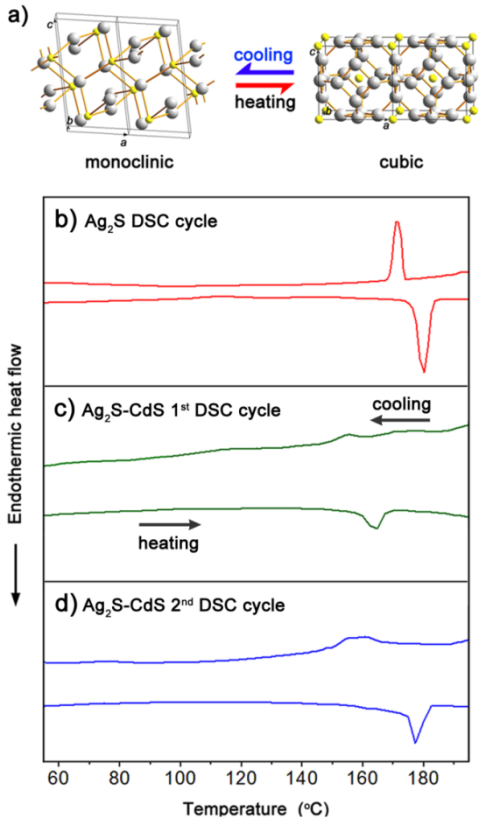

Fig. 7 (a) Schematic illustration of the structure phase transition between monoclinic and cubic Ag_2S. (b–d) DSC heating/cooling curves of (b) pure Ag_2S nanocrystals and (c,d) Ag_2S catalytic heads for the first and second cycle, respectively. The Ag_2S catalytic heads used for DSC measurements are from Ag_2S-CdS matchstick-like heteronanostructures prepared at 1:2 Ag/Cd molar ratio.

Fig. 7b dispalys the DSC heating/cooling cycle curve for pure Ag_2S nanocrystals (~27.5 nm in the mean diameter, Fig. S2†), in which an endothermic peak at 180 °C and an exothermal peak at 172 °C are detected. This result indicates that the structural transitions between monoclinic and cubic structures of Ag_2S nanocrystals occur at these temperatures. The transition temperature of 180 °C of the monoclinic-cubic phase measured for the pure Ag_2S nanocrystals is well consistent with the values in the literature.[31,32,44,45]

However, Ag_2S catalyst heads exhibit a different phase transformation behavior. As shown in Fig. 7c, an endothermic peak at 164 °C and an exothermal peak at 155 °C are observed in the first DSC heating/cooling cycle between 0 °C and 200 °C, which means that Ag_2S catalyst heads transform from monoclinic structure to cubic structure at 164 °C and then return to monoclinic structure at 155 °C. Obviously, the monoclinic-cubic phase transition temperature of the Ag_2S catalyst heads is decreased by 16 °C compared to that of the pure Ag_2S nanocrystals (Fig. 7b). Importantly, it is measured that the endothermic peak at 164 °C of Ag_2S catalyst heads has an onset temperature at 159 °C (Fig. S3†), that is to say, Ag_2S catalyst heads start to transform to cubic structure at 159 °C. In our synthesis, the reaction temperature is fixed at 160 °C and is higher than 159 °C. Therefore, we can conclude that at the synthetic temperature of 160 °C Ag_2S catalyst nanocrystals are in the superionic-state cubic phase, which actually catalyzes the growth of CdS nanorods.[30] Fig. 7c shows that the DSC endothermic and exothermal peaks for Ag_2S catalyst heads display a weak intensity, compared to that for the pure Ag_2S nanocrystals (Fig. 7b). This is because a large amount of CdS stem component coexists with Ag_2S catalyst heads.

Furthermore, it is found that the DSC heating process caused significant damage to the Ag_2S-CdS matchstick-shaped heteronanostructures and accordingly caused the change of phase transition behavior of Ag_2S catalyst heads. As shown in Fig. 7d, the second DSC cycle reveals that the monoclinic-cubic phase transition temperature of Ag_2S increases to 177 °C from 164 °C detected in the first DSC cycle. Under our TEM studies (Fig. S4†), the sintering and agglomeration of the sample were observed after the first heating/cooling cycle, which leads to the size increase and the shape change of Ag_2S catalyst heads. The size increase of Ag_2S catalyst heads will cause an increase in the transition temperature of Ag_2S, like the behavior found in Cu_2S nanocrystals.[46a]

Along with the DSC analyses, the crystal phase transition of Ag_2S is also examined by the variable-temperature XRD measurements. Fig. 8 shows the temperature-dependent XRD patterns of pure Ag_2S nanocrystals (Fig. S2). It can be seen that, with the increase of temperature, Ag_2S clearly undergoes a structural transition from the low-temperature monoclinic phase (JCPDS# 89-3840, a = 4.23 Å, b = 6.91 Å, and c = 7.87 Å) to the high-temperature cubic phase (JCPDS# 71-0995, a = 4.86 Å). The transition temperature is measured between 170 and 190 °C, consistent with the value detected in the DSC curve (Fig. 7b). The variable-temperature XRD measurements were also taken on the sample of Ag_2S-CdS matchstick-like

heteronanostructures (Ag/Cd = 1:2). However, the change in the diffraction peaks of Ag_2S heads is not clearly observed because the weak peak intensity of Ag_2S and the peak overlap of Ag_2S with CdS in the temperature-dependent XRD patterns. It is believed that Ag_2S catalytic heads exhibits a phase change behavior similar to the pure Ag_2S nanocrystals, except that the transition temperature is different.

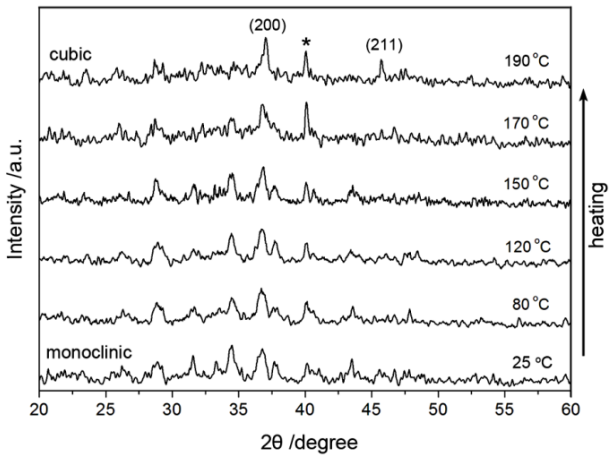

Fig. 8 Temperature-dependent XRD patterns of as-prepared pure Ag2S nanocrystals. The peak marked with an asterisk (d = 2.24 Å, 2θ = 40.05°) is derived from instrument and cannot be assigned.[30]

Above the phase transition temperature, Ag_2S nanocrystals are in the superionic phase and possess a large number of cation vacancies and a high mobility of cations (Ag^+) in the body-centered cubic sublattice of S^{2-} ions.[31,32] These structural characteristics help Ag_2S nanocrystals to display good ability to catalyze the growth of CdS nanorods. As reported previously, the high-density Ag^+ vacancy sites are favorable for the occupation of Cd ions over Ag^+ vacancy sites and then the dissolution of Cd ions in Ag_2S catalytic nanocrystals,[21,23,27,30] and meanwhile, the highly mobile Ag^+ ions can enhance the growth rate of CdS nanorods.[21,30]

In view of the crystal phase change of Ag_2S catalyst at different temperatures, the synthetic temperature plays an important role in the formation of Ag_2S-CdS matchstick-like heteronanostructures. At 140 °C, which is below the transition temperature of superionic-phase Ag_2S, Ag_2S catalyst particles are usually in the monoclinic phase, but they could also be in the superionic-conductor cubic phase in accordance with the influence of particle size on the crystal phases and phase transition temperature.[46] In this case, there will be a mixture of separated Ag_2S nanoparticles and Ag_2S-CdS matchstick-like heteronanostructures in the products (Fig. S5a†). At the temperatures higher than the onset temperature (159 °C, detected by DSC) of phase transition, for example, 160 and 180 °C, Ag_2S is in the superionic cubic phase and thus can effectively catalyse the growth of CdS nanorods to form Ag_2S-CdS matchstick-shaped heteronanostructures. However, 180 °C is high enough to cause the thermal decomposition of $Cd(DDTC)_2$ and yield the thin CdS nanorods in the products (Fig. S5b†). So, it is clear that 160 °C is a very suitable temperature for the synthesis of Ag_2S-CdS matchstick-like heteronanostructures (Fig. 3).

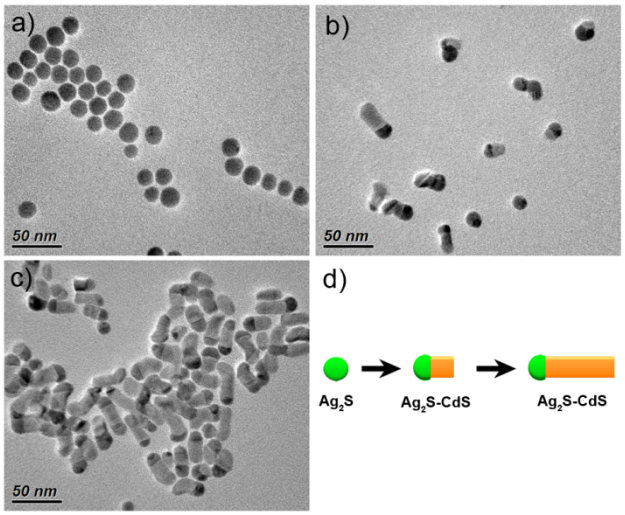

Fig. 9 Growth process of the Ag_2S-CdS matchstick-like heteronanostructures (Ag/Cd = 1:2, 160 °C) at various stages: (a) Ag_2S catalytic seeds; (b) 2 min; (c) 10 min. (d) Schematic illustration for the above growth process with prolonging reaction time.

The catalytic role of Ag_2S nanoseeds in the formation of CdS nanorods can be demonstrated by monitoring the morphological evolution of Ag_2S-CdS heteronanostructures (Ag/Cd = 1:2) at different growth stages by means of TEM. The results are shown in Fig. 9. At the initial stage, spherical Ag_2S nanocrystals (Fig. 9a, prepared from 0.1 mmol $AgNO_3$ at 160 °C for 20 min) served as catalytic seeds. After adding $Cd(DDTC)_2$ for 2 min, the products show a biphasic heterostructure composed of darker Ag_2S and lighter CdS and the CdS part has a tendency to grow into rod-like shape (Fig. 9b). With further growth of CdS for 10 min, almost all the products are Ag_2S-CdS matchstick-like heterostructures with a longer CdS nanorod (Fig. 9c). From these TEM observations, it can also be seen the shape of Ag_2S seeds become from spherical to hemispherical, and that the diameter size of Ag_2S heads is slightly larger than that of CdS nanorods at their interfaces. Such characteristics, which are often observed in a nanowire catalytic growth mechanism,[14–16,23–30] indicate that the formation of Ag_2S-CdS matchstick-like heteronanostructures follows a catalytic growth route. The above growth process with reaction time increasing can be clearly illustrated in Fig. 9d.

As indicated in Fig. 1, the Ag_2S-CdS phase diagram shows a peritectic temperature at 893 °C and below this temperature Ag_2S and CdS are solid. So, Ag_2S seeds can be simply seen as a solid-state catalyst when the CdS rod-like nanocrystal growth proceeds at the synthetic temperature of 160 °C, like Ag_2Se solid-state catalyst for the ZnSe nanowire growth, where we suggested a solution-solid-solid (SSS) catalytic mechanism.[30] The formation process of Ag_2S-CdS matchstick-shaped heteronanostructures (Fig. 9) can be rationally explained by the

SSS growth model. Firstly, the occupation of Cd^{2+} over Ag^{+} vacancy sites in Ag_2S is a dissolution process of Cd^{2+} in Ag_2S, which will lead to the formation (nucleation) of CdS species within Ag_2S catalysts. Then, with the CdS species aggregating, the new phase of CdS will be readily precipitated out from Ag_2S nanocatalysts because the supersaturation of CdS in Ag_2S is easily achieved due to the low solubility of CdS in the Ag_2S (the red region in Fig. 1). As the reaction proceeds, the new phase of CdS will eventually grow into nanorods by the catalysis of Ag_2S. Because the solubility product constant (K_{sp}) of Ag_2S is much lower than that CdS (K_{sp}: 6.3×10^{-50}(Ag_2S) << 8.0×10^{-27}(CdS))[47], it is difficult for Cd^{2+} to replace Ag^{+} ions in Ag_2S catalytic nanocrystals. Meanwhile, Ag_2S has a low solubility in CdS, which suppresses the consuming of Ag_2S nanocrystals during the growth of CdS nanorods. These two reasons ensure the remaining of Ag_2S nanocrystals at the end of CdS nanorods to construct the matchstick-like Ag_2S-CdS heteronanostructures.

4. Conclusions

We have demonstrated the solution-phase catalytic synthesis of Ag_2S-CdS heteronanostructures with a matchstick-like shape. The control over the diameter of Ag_2S heads and the length of CdS stems is realized by tuning the molar ratios of Ag/Cd precursors. The structural transition of Ag_2S catalytic nanocrystals is investigated, which confirms that the high-temperature superionic conductor phase Ag_2S catalyze the growth of CdS nanorods (stems). It is suggested that the structural characteristics of superionic conductor phase and the low solubility of CdS in Ag_2S endow Ag_2S nanocrystals with good catalytic ability to grow CdS nanorods. Meanwhile, the formation of Ag_2S-CdS matchstick-like heteronanostructures has been reasonably clarified through the SSS catalysed growth mechanism, where superionic phase Ag_2S nanoseeds act as catalyst and remain at one end of CdS nanorods to form matchstick-like Ag_2S-CdS heteronanostructures. This work provides a convenient strategy for controlled preparation of 1D heteronanostructures containing two dissimilar metal chalcogenides, which may be useful for engineering the composition and band gap of semiconductor nanostructures with interesting optical properties or multifunctionality.

Acknowledgements

The authors are grateful to the support for this research from the National Natural Science Foundation of China (NSFC: 21201086, 21071136, 51271173, 61006049), the National Basic Research Program of China (2010CB934700, 2012CB932001), the Ministry of Science and Technology of China (2009DFA50620, 2011DFG52970), the Ministry of Education of China (IRT1064), Jiangsu Innovation Research Team, and the Research Foundation of Jiangsu University (11JDG071).

Notes and references

[a]Functional Molecular Materials Research Centre, Scientific Research Academy & School of Chemistry and Chemical Engineering, Jiangsu University, Zhenjiang 212013, P. R. China. E-mail: junleewang@yahoo.com or wangjl@mail.ujs.edu.cn; Fax: +86 511 88797815

[b]Hefei National Laboratory of Physical Sciences at the Microscale & Department of Chemistry, University of Science and Technology of China (USTC), Hefei 230026, P. R. China. E-mail: qyoung@ustc.edu.cn

[c]School of Materials Science & Engineering, Jiangsu University, Zhenjiang 212013, P. R. China

†Electronic Supplementary Information (ESI) available: XRD pattern, TEM images and DSC curve (Figs. S1–S5). See DOI: 10.1039/b000000x/

1 R. Costi, A. E. Saunders and U. Banin, *Angew. Chem., Int. Ed.,* 2010, **49**, 4878–4897.

2 L. Carbone and P. D. Cozzoli, *Nano Today*, 2010, **5**, 449–493.

3 S. E. Habas, H. Lee, V. Radmilovic, G. A. Somorjai and P. Yang, *Nat. Mater.,* 2007, **6**, 692–697.

4 H. Yu, M. Chen, P. M. Rice, S. X. Wang, R. L. White and S. Sun, *Nano Lett.,* 2005, **5**, 379–382.

5 T. Mokari, E. Rothenberg, I. Popov, R. Costi and U. Banin, *Science,* 2004, **304**, 1787–1790.

6 Q. Tian, J. Hu, Y. Zhu, R. Zou, Z. Chen, S. Yang, R. Li, Q. Su, Y. Han and X. Liu, *J. Am. Chem. Soc.,* 2013, **135**, 8571–8577.

7 S. Shen, Y. Zhang, L. Peng, Y. Du and Q. Wang, *Angew. Chem., Int. Ed.,* 2011, **50**, 7115–7118.

8 J. Zhang, Y. Tang, K. Lee and M. Ouyang, *Science,* 2010, **327**, 1634–1638.

9 K.-W. Kwon and M. Shim, *J. Am. Chem. Soc.,* 2005, **127**, 10269–10275.

10 D. A. Chen, F. Zhao, H. Qi, M. Rutherford and X. Peng, *Chem. Mater.,* 2010, **22**, 1437–1444.

11 S. Deka, A. Quarta, M. G. Lupo, A. Falqui, S. Boninelli, C. Giannini, G. Morello, M. De Giorgi, G. Lanzani, C. Spinella, R. Cingolani, T. Pellegrino and L. Manna, *J. Am. Chem. Soc.,* 2009, **131**, 2948–2958.

12 M. Saruyama, Y.-G. So, K. Kimoto, S. Taguchi, Y. Kanemitsu and T. Teranishi, *J. Am. Chem. Soc.,* 2011, **133**, 17598–17601.

13 M. D. Regulacio, C. Ye, S. H. Lim, M. Bosman, L. Polavarapu, W. L. Koh, J. Zhang, Q. H. Xu and M. Y. Han, *J. Am. Chem. Soc.,* 2011, **133**, 2052–2055.

14 L. J. Lauhon, M. S. Gudiksen, D. Wang and C. M. Lieber, *Nature*, 2002, **420**, 57–61.

15 M. Hocevar, G. Immink, M. Verheijen, N. Akopian, V. Zwiller, L. Kouwenhoven and E. Bakkers, *Nat. Commun.,* 2012, **3**, *1266*.

16 L. Ouyang, K. N. Maher, C. L. Yu, J. McCarty and H. Park, *J. Am. Chem. Soc.,* 2007, **129**, 133–138.

17 S. Kudera, L. Carbone, M. F. Casula, R. Cingolani, A. Falqui, E. Snoeck, W. J. Parak and L. Manna, *Nano Lett.,* 2005, **5**, 445–449.

18 S. Deka, A. Falqui, G. Bertoni, C. Sangregorio, G. Poneti, G. Morello, M. De Giorgi, C. Giannini, R. Cingolani, L. Manna and P. D. Cozzoli, *J. Am. Chem. Soc.,* 2009, **131**, 12817–12828.

19 R. Buonsanti, V. Grillo, E. Carlino, C. Giannini, F. Gozzo, M. Garcia-Hernandez, M. A. Garcia, R. Cingolani and P. D. Cozzoli, *J. Am. Chem. Soc.,* 2010, **132**, 2437–2464.

20 S. H. Choi, E. G. Kim and T. Hyeon, *J. Am. Chem. Soc.,* 2006, **128**, 2520–2521.

21 S. T. Connor, C.-M. Hsu, B. D. Weil, S. Aloni and Y. Cui, *J. Am. Chem. Soc.,* 2009, **131**, 4962–4966.
22 J.-Y. Chang and C.-Y. Cheng, *Chem. Commun.,* 2011, **47**, 9089–9091.
23 W. Han, L. Yi, N. Zhao, A. Tang, M. Gao and Z. Tang, *J. Am. Chem. Soc.,* 2008, **130**, 13152–13161.
24 L. Yi, A. Tang, M. Niu, W. Han, Y. Hou and M. Gao, *CrystEngComm,* 2010, **12**, 4124–4130.
25 H. Ye, A. Tang, L. Huang, Y. Wang, C. Yang, Y. Hou, H. Peng, F. Zhang and F. Teng, *Langmuir,* 2013, **29**, 8728–8735.
26 (a) T. You, J. Wang, H. Feng, K. Chen, W. Fan, C. Zhang and R. Miao, *Dalton Trans.*, 2013, **42**, 7724–7730; (b) J. L. Wang, T. T. You, H. Feng, K. M. Chen and B. Xu, *J. Cryst. Growth*, 2013, **374**, 60–64.
27 G. Zhu and Z. Xu, *J. Am. Chem. Soc.*, 2011, **133**, 148–157.
28 Z. Huang, P. Zhong, M. Li, F. Tian and C. Zhang, *Nanotechnology,* 2012, **23**, 335604.
29 (a) S. Shen, Y. Zhang, Y. Liu, L. Peng, X. Chen and Q. Wang, *Chem. Mater.*, 2012, **24**, 2407−2413; (b) S. Shen and Q. Wang, *Chem. Mater.*, 2013, **25**, 1166−1178; (c) S. Shen, Y. Zhang, L. Peng, B. Xu, Y. Du, M. Deng, H. Xu and Q. Wang, *CrystEngComm*, 2011, **13**, 4572–4579.
30 J. Wang, K. Chen, M. Gong, B. Xu and Q. Yang, *Nano Lett.,* 2013, **13**, 3996−4000.
31 S. Hoshino, *Solid State Ionics,* 1991, **48**, 179–201.
32 M. Kobayashi, *Solid State Ionics,* 1990, **39**, 121–149.
33 Y. Du, B. Xu, T. Fu, M. Cai, F. Li, Y. Zhang and Q. Wang, *J. Am. Chem. Soc.,* 2010, **132**, 1470–1471.
34 P. Peng, B. Sadtler, A. P. Alivisatos and R. J. Saykally, *J. Phys. Chem. C,* 2010, **114**, 5879–5885.
35 S. Mourdikoudis and L. M. Liz-Marzán, *Chem. Mater.,* 2013, **25**, 1465–1476.
36 I. D. Olekseyuk, O. V. Parasyuk, V. O. Halka, L. V. Piskach, V. Z. Pankevych and Ya. E. Romanyuk, *J. Alloys Compd.,* 2001, **325**, 167–179.
37 Y. Wang, V. Schmidt, S. Senz and U. Gösele, *Nat. Nanotechnol.,* 2006, **1**, 186–189.
38 C. Y. Wen, M. C. Reuter, J. Bruley, J. Tersoff, S. Kodambaka, E. A. Stach and F. M. Ross, *Science,* 2009, **326**, 1247–1250.
39 F. D. Wang, A. Dong, J. Sun, R. Tang, H. Yu and W. E. Buhro, *Inorg. Chem.,* 2006, **45**, 7511–7521.
40 H. Shen, H. Shang, J. Niu, W. Xu, H. Wang and L. S. Li, *Nanoscale,* 2012, **4**, 6509–6514.
41 G. Hota, S. B. Idage and K. C. Khilar, *Colloid Surf. A: Physicochem. Eng. Asp.,* 2007, **293**, 5–12.
42 J. F. Moulder, W. F. Stickle, P. E. Sobol and K. D. Bomben, in *Handbook of X-ray Photoelectron Spectroscopy*, ed. J. Chastain and R. C. King, Physical Electronics, Inc., 1995, pp. 60–61.
43 See: http://srdata.nist.gov/xps/main_search_menu.aspx.
44 C. Xiao, J. Xu, K. Li, J. Feng, J. Yang and Y. Xie, *J. Am. Chem. Soc.*, 2012, **134**, 4287–4293.
45 N. E. Pingitore, B. F. Ponce, L. Estrada, M. P. Eastman, H. L. Yuan, L. C. Porter and G. Estrada, *J. Mater. Res.,* 1993, **8**, 3126–3130.
46 (a) J. B. Rivest, L.-K. Fong, P. K. Jain, M. F. Toney and A. P. Alivisatos, *J. Phys. Chem. Lett.,* 2011, **2**, 2402–2406; (b) A. Sahu, L. Qi, M. S. Kang, D. Deng and D. J. Norris, *J. Am. Chem. Soc.*, 2011, **133**, 6509–6512.
47 J. A. Dean, in *Lange's Handbook of Chemistry*, Mc Graw-Hill Inc., 15th edn. 1999, Section 8, Table 8.6.

TOC entry

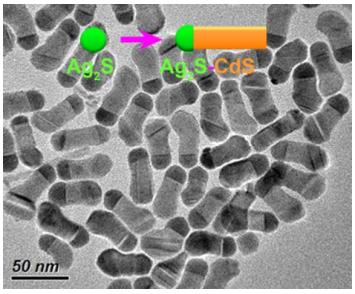

Ag_2S nanocrystals are catalytically active to grow CdS nanorods in oleylamine, and remain at their end to yield Ag_2S-CdS matchstick-like heteronanostructures.